NUMERICAL INVESTIGATION OF AN ANISOTHERMAL TURBULENT FLOW WITH EFFUSION

Simon Mendez
CFD Team, CERFACS
42, avenue Gaspard Coriolis. 31057 Toulouse cedex 1, France
mendez@cerfacs.fr

Franck Nicoud
Département de Mathématiques CNRS UMR 5149 - CC51,
University Montpellier II
Place Eugène Bataillon 34095 Montpellier cedex 5, France
nicoud@math.univ-montp2.fr

ABSTRACT

The results of a Large-Eddy Simulation of the flow around a perforated plate are described. A temperature difference is imposed across the perforated plate, to study the effusion cooling process. A configuration of full-coverage film cooling is considered: a specific methodology allowing to perform the simulation in a periodic computational domain is presented. The geometry corresponds to classical configurations encountered in gas turbines liners: the hole diameter is $0.5\,mm$, the thickness of the plate $1\,mm$, and the hole is angled at 30° respect to the plate. The density ratio is 2.85 and the blowing ratio is $M = 1$. The flow obtained in such a periodic domain is described, focusing on information relevant to the estimation of mass/momentum/energy fluxes through the plate.

CONTEXT

In gas turbines, the turbine blades and the liner of the combustion chamber are submitted to large thermal constraints. As the materials used for these solid parts cannot stand such high temperature and temperature gradients, they need to be cooled. As pointed out by Lefebvre (1999), the most efficient cooling system would be transpiration-based: the solid parts to be cooled would be made of porous material through which cool air would be injected. The resulting uniform film of fresh gas would isolate the solid parts from the hot products. However, the application of transpiration in gas turbines is not practical due the mechanical weakness of available porous materials and alternative technological solutions are sought for. One alternative is the so-called full-coverage film cooling (FCFC) technique, where the liner is a multi-perforated plate with thousands of submillimetric angled holes. The air flowing in the casing is injected through the perforations, as shown in Fig. 1. The resulting jets coalesce and form an isolating film protecting the internal face of the liner from hot burnt gases.

For economical reasons, computational fluid dynamics is now widely used as a design tool by combustion chamber manufacturers. However, despite the increasing power of the computers, the number of submillimetric holes is far too large to allow a complete description of the jets when performing 3D turbulent reacting simulations of the burner. Effusion is however known to have drastic effects on the whole flow structure, notably by changing the flame position. As a consequence, appropriate wall models have to be developed to account for effusion cooling in predictive full-scale computations.

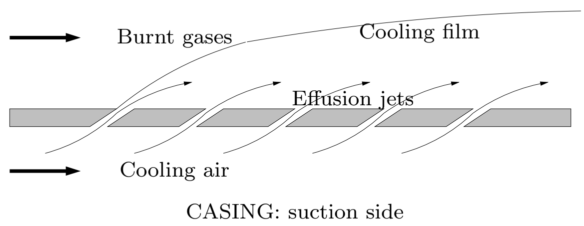

Figure 1: Principle of full-coverage film cooling: fresh air flowing in the casing is injected into the combustion chamber through the liner perforations.

The design of such models needs to be supported by detailed data concerning FCFC. Such detailed description of the flow in the near wall region can hardly be obtained experimentally because a) the perforation imposes small-scale structures that are out of reach of current experimental devices b) the thermal conditions in actual gas turbines make any measurement very challenging; consequently, most available measurements deal with large-scale isothermal flows (see for example Yavuzkurt *et al.*, 1980, Gustafsson, 2001, Miron, 2005). On the other hand, Large-Eddy Simulations (LES) has proved to be adapted to film cooling configurations (Tyagi and Acharya, 2003, Iourokina and Lele, 2006 and Renze *et al.*, 2006). However, the reported studies deal with geometries including only one row of perforations, which is typical of blade film cooling. Therefore, a specific methodology has to be developed to study FCFC. Recently, the case of a large-scale isothermal FCFC configuration has been studied with LES using an original approach (see Mendez *et al.*, 2006a, 2006b): the computational domain contains only one perforation and periodic boundary conditions are applied in the directions parallel to the perforated plate. This method has provided convincing results when compared to the reference experimental results of Miron (2005). This paper details the extension of this method to anisothermal configurations. The complete description of the numerical methodology is provided in the next section and the computational results are described afterwards.

NUMERICAL DETAILS

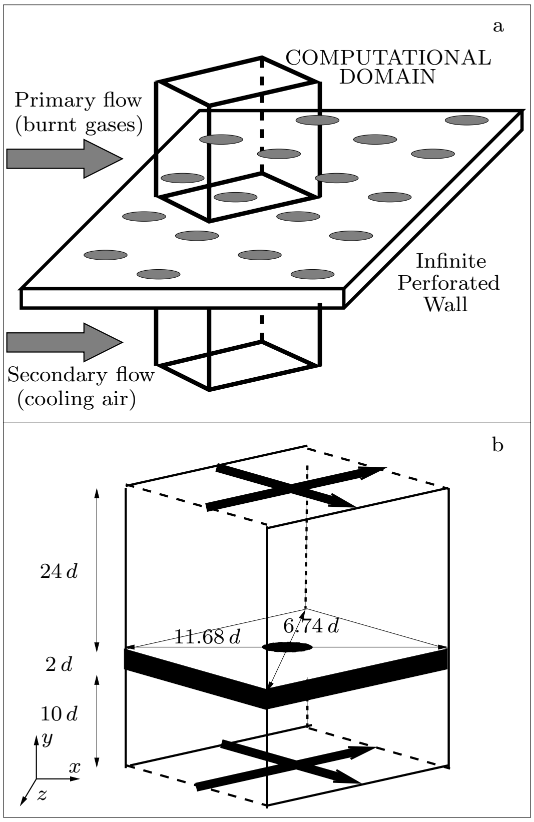

Figure 2: From the infinite plate to the 'bi-periodic' calculation domain. **a**: Geometry of the infinite perforated wall. **b**: Calculation domain centered on a perforation; the bold arrows correspond to the periodic directions. The dimensions of the computational domain are provided.

The CPU time required for performing a LES of a classical multi-perforated plate with hundreds of jets would be prohibitive. An infinite perforated plate is then considered, so that the calculation domain can be reduced to a periodic unit box containing a unique perforation. The perforated plate separates the domain into two parts: one containing burnt gases (top part, primary flow), the other containing cooling air (bottom part, secondary flow). As shown in Fig. 2, periodic conditions are imposed along the directions parallel to the plate to reproduce the geometry of an infinite plate.

The main tangential flow at both sides of the plate is enforced thanks to a constant source term added to the momentum equation, as it is usually done in channel flow simulations. In order to sustain the effusion flow through the hole, a uniform vertical mass flow rate is imposed at the bottom boundary of the domain. The numerical strategy has first been tested in an isothermal case by computing a typical operating point of the LARA experiment (see Miron, 2005) developed at TURBOMECA (SAFRAN group). Numerical results compare favorably with experimental measurements (Mendez *et al.*, 2006a) and depend neither on the numerics (the CERFACS and the Stanford/CTR LES codes provide very close results) nor on the size of the domain (1-hole and 4-hole computations give similar results, see Mendez *et al.*, 2006b).

To adapt this methodology to anisothermal calculations, a constant source term is applied on the upper channel (hot side) to heat the fluid and compensate the constant cooling imposed by the injection of cold gas through the hole. The liner being assumed thermally thin, its temperature T_{wall} is considered to be uniform and fixed *a priori* (known from experimental results for example). The amplitude of the source term is then tuned so that the surface integral of the heat flux entering the solid is null. In doing so, the statistically steady state of the turbulent flow is consistent with the constant uniform temperature prescribed for the liner. The source term is uniform over the region where the temperature increases from T_{wall} to the temperature value prescribed for the burnt gases.

All simulations are carried out with the LES code named AVBP (www.cerfacs.fr/cfd/avbp_code.php) and developed at CERFACS. It solves the compressible Navier–Stokes equations on unstructured meshes for the conservative variables (mass density, momentum and total energy). AVBP is dedicated to LES and DNS and has been widely used and validated in the past years in all kinds of configurations (Schönfeld and Rudgyard, 1999, Schmitt *et al.*, 2007), and notably in jets in crossflow cases (Priere *et al.*, 2004). Simulations are based on the WALE sub-grid model (Nicoud and Ducros, 1999). The numerical scheme is the TTGC scheme (Colin and Rudgyard, 2000): this essentially non-dissipative scheme was specifically developed to handle unsteady turbulent flows. It is third order accurate in both space and time.

The geometry of the calculation domain is detailed in Fig. 2b, where the dimensions are provided. The origin (0,0,0) is located at the center of the hole exit. The hole diameter is $d = 0.5\,mm$, the plate thickness is $h = 1\,mm$. The hole is inclined in the streamwise direction (the angle between the wall and the hole direction is $\alpha = 30°$). The top and bottom boundaries of the domain are located respectively at 10 and 24 hole diameters from the plate. The computational domain is diamond-shaped, which corresponds to the staggered arrangement of the perforations in a combustion chamber. The spacing between the holes corresponds to classical industrial applications: the distance between two rows of holes is 5.84 diameters in the streamwise direction and 3.37 diameters in the spanwise direction. Due to the staggered disposition of the perforations, the hole-to-hole distances are 2×5.84 and 2×3.37 diameters in the streamwise and spanwise directions respectively.

The calculation grid contains 2,050,000 tetrahedral cells: fifteen points describe the diameter of the hole and on the average the first off-wall point is located 10 wall units apart from the wall in the injection side and 5 wall units apart from the wall in the suction side. Typically the cells along the wall and in the hole are sized to a height of $0.03\,mm$ (recall that the aperture diameter is $0.5\,mm$).

ANISOTHERMAL CALCULATIONS

This paper aims at presenting the simulations performed in an anisothermal case, with a large temperature difference between the hot and the cold sides of the domain. The operating point corresponds to an anisothermal full-scale experiment conducted by Rouvreau (2001). The temperature is from $T_{cold} = 330\,K$ for the cooling fluid to $T_{hot} = 873\,K$ on the hot side, the temperature of the liner being equal to $T_{wall} = 455\,K$. The pressure in the bottom channel is $P_{cold} = 208000\,Pa$ and the pressure drop ΔP through the plate is 4% of P_{cold}. The resulting bulk momentum in the hole is $(\rho V)_{jet} = 128\ kg\,m^{-2}\,s^{-1}$. The corresponding discharge coefficient is approximately $C_D = 0.72$ (with $\Delta P\, {C_D}^2 = \frac{1}{2}\rho_{jet} {V_{jet}}^2$). The Reynolds numbers of the crossflows (based on far-field flow rates and the height where

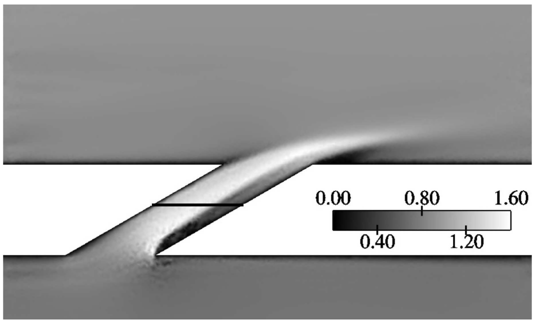

Figure 3: Momentum magnitude over the cutting plane located at $z = 0$. Black line: location of the cutting plane displayed in Fig. 4 and 6.

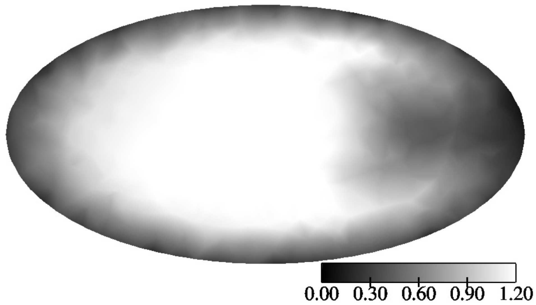

Figure 4: Streamwise momentum over the cutting plane located at $y = -d$ (see Fig. 3).

the temperature recovers the characteristic temperature of the corresponding crossflow) are respectively 6000 and 7900 for the cold and the hot sides. The Reynolds number in the hole (based on the hole diameter, bulk flow rate and viscosity through the aperture) is 3200 and the blowing ratio (ratio of the jet momentum on the hot flow momentum) is close to 1.

In the following sections, the displayed results are dimensionless. The reference momentum is $(\rho V)_{jet}$, and temperature is displayed as $T^* = \dfrac{T - T_{hot}}{T_{cold} - T_{hot}}$. At the wall, $T^* = 0.77$. All results are time-averaged over a period corresponding to 80 flow through times based on the hot crossflow velocity and the streamwise hole-to-hole distance.

Figure 3 displays the momentum magnitude field over the cutting plane $z = 0$. The classical topology of film cooling flows is reproduced: cooling fluid coming from the bottom channel is aspired through the hole due to the pressure drop and injected in the upper channel. At the entrance of the aperture, the flow separates, due the sharp edge. This separation is a classical feature of film cooling with inclined holes (see for example Iourokina and Lele, 2006). It is responsible for the classical kidney form of the jet in the aperture, as seen in Fig. 4 on the streamwise momentum field at half the height of the aperture (the displayed plane is represented by a black line in Fig. 3). Note that at the outlet of the hole, the blowing ratio is high enough to make the jet separate from the wall.

The temperature field over the cutting plane $z = 0$ is shown in Fig. 5. On the suction side of the plate, a thin thermal boundary layer develops, due to higher temperature of the liner. This boundary layer is submitted to the suction due to the hole. The temperature at the inlet of the hole is then different from the cooling temperature. Thermal convection is also present in the hole itself, where the aver-

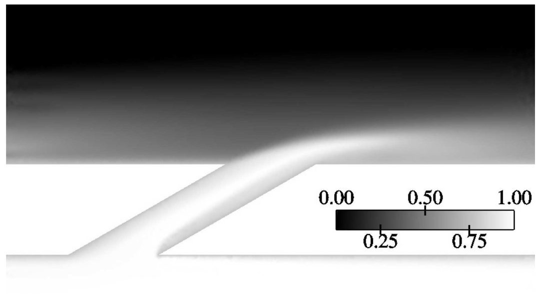

Figure 5: Temperature over the cutting plane located at $z = 0$. Temperature is from 0, in the hot gases, to 1 in the cold gases.

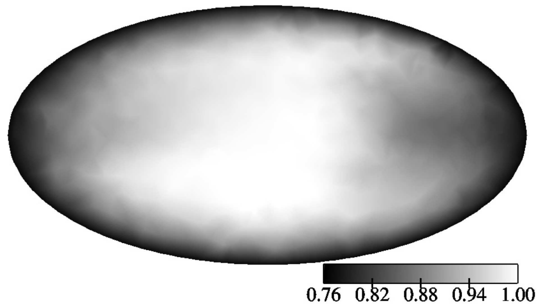

Figure 6: Temperature over the cutting plane located at $y = -d$ (see Fig. 3).

aged temperature of the cooling fluid continues to increase. In the aperture, the temperature is higher than T_{cold} in two zones: near the upstream wall, where the influence of the aspired boundary can be observed, and near the downstream wall, in the low-momentum region. This is also observed in Fig. 6, where the temperature is displayed over the cutting plane located at half the height of the aperture (see Fig. 3 for the location of the plane).

The reported simulation provides interesting information relevant to anisothermal film cooling flows:

- Heat flux at the wall (hot side, cold side and in the hole),
- Comparison of the pressure losses in the anisothermal and isothermal cases,
- Influence of the variations of density on the aerodynamic behavior of the jet.

Assessment of the heat transfers

Computations provide local information about the heat transfers at the wall. As previously said, the source term that heats the flow in the hot part of the computational domain is tuned so that the perforated plate reaches the thermal equilibrium: the integral of the heat flux over the total surface of the plate is null. The heat flux is always positive on the suction side and in the aperture (the fluid is colder than the plate) and globally negative on the injection side. Computations show that the heat transfer in the hole is not negligible, as the integral of the heat flux over the hole surface, $< q_{hole} >$, is approximately 45% of the integral of the heat flux over the suction side surface , $< q_{cold} >$, although the hole surface is much smaller.

Figures 7 and 8 show the local Nusselt number over the suction and injection sides of the plate respectively. The Nusselt number displayed here is based on the hole diameter and on the wall and cooling temperature difference:

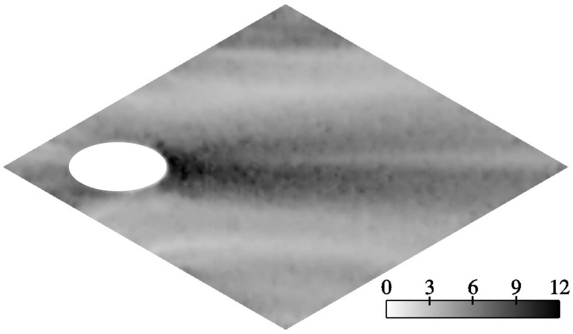

Figure 7: Nusselt number over the suction plane ($y = -2d$).

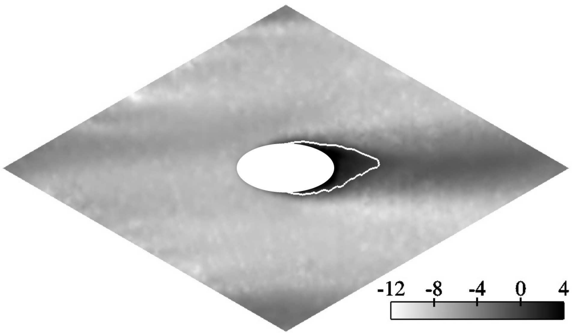

Figure 8: Nusselt number over the injection plane ($y = 0$). The contour $Nu = 0$ is represented thanks to the white line.

$Nu = \dfrac{q\,d}{\lambda(T_{wall} - T_{cold})}$, where q is the local heat flux $q = -\lambda \left[\dfrac{\partial T}{\partial y}\right]_{wall}$ and λ is the thermal conductivity of the gas at T_{wall} ($\lambda = 0.033\ W.m^{-1}.K^{-1}$).

The Nusselt field over the suction side of the perforated plate can be easily interpreted, keeping in mind the main feature of the flow in the suction channel: the aspiration of the thermal boundary layer created by the exchanges between the cooling fluid and the hot plate. The effect of aspiration is mainly visible in the wake of the hole: immediately downstream of the aperture entrance, the heat flux is maximum. Then, it decreases with the streamwise distance, as the thickness of the boundary layer increases (Fig. 5). Outside the hole wake, the heat transfers are much smaller. These zones are also regions of low velocity, where the dynamical and thermal boundary layers are much thicker.

Regarding the injection side of the plate, positive and negative values of the Nusselt number are observed. Over the major part of the plate, the heat flux is negative, the plate being heated by the main flow. A quasi-constant value of $Nu \approx -8$ is measured over the injection face of the plate. The inhomogeneity of the heat transfers on this face of the plate is due to the jet: the plate is cooled by the flow in a region just downstream of the hole. As shown by the white iso-line $Nu = 0$, this region is very small. Indeed, the jet core, where the lowest temperatures are observed, penetrates in the main stream and does not remain attached near the perforated plate. However, the jet has a huge influence on the heat transfers by decreasing the fluid temperature downstream of the hole outlet. In the wake of the jet, heat transfers are considerably reduced. Figure 8 also shows the presence of two small bands of higher heat transfers ($Nu \approx -10$) on both sides of the hole wake. It is the consequence of two counter-rotating vortices that entrain the hot fluid towards the plate, increasing the near-wall temperature gradients. These vortices are discussed in the next section.

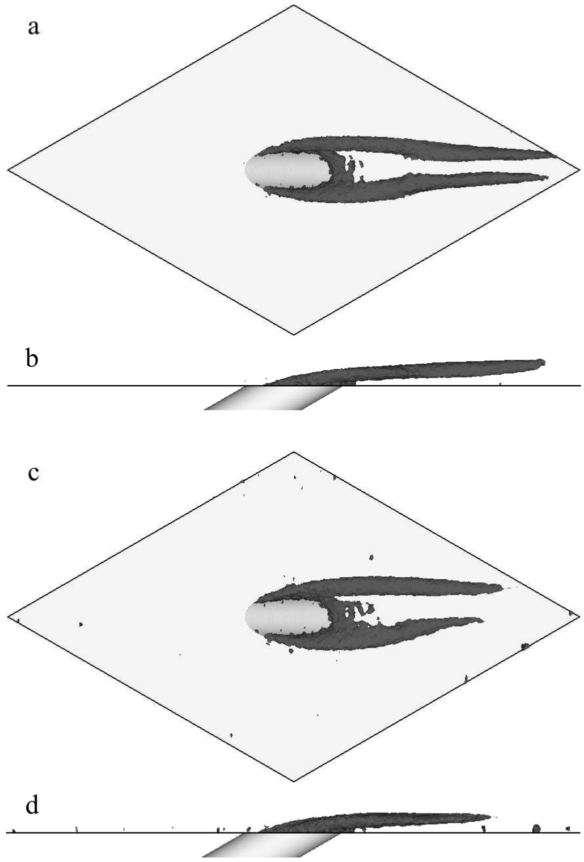

Figure 9: Visualization of the CVP: top (a and c) and side (b and d) views of an iso-surface of Q-criterion. **a, b**: isothermal case. **c, d**: anisothermal case.

Effect of density variations

The objective of this section is to evaluate the impact of density variations on the flow, by comparing anisothermal and isothermal calculations for the same geometry. The simulation presented above is compared with a simulation in an isothermal case: to perform the isothermal computation, the wall temperature is set to the cold temperature, $T_{wall} = 330\,K$, and the source term that heats the flow is set to zero. The pressure difference is maintained. The resulting blowing ratio is 1, as in the anisothermal calculation, and the density ratio is 1.

Pressure losses do not seem to be affected by density variations. The discharge coefficient C_D is 0.77 in the isothermal case and 0.76 in the anisothermal case. This is consistent with the results of Champion *et al.* (2005), who measured discharge coefficients through a multi-perforated plate in an anisothermal configuration with holes inclined at 18.5°. They found that C_D only depends on the Reynolds numbers in the hole and in the suction side of the plate. The Reynolds numbers are similar in the isothermal and anisothermal cases, leading to identical values of discharge coefficients. However, the mass flow rate through the plate is 8 % higher in the isothermal calculation ($(\rho V)_{jet} = 138$ $kg\,m^{-2}\,s^{-1}$).

The impact of density variations on the topology of the flow is now discussed. The main vortical structure observed in the jet (injection side of the plate) is the counter-rotating

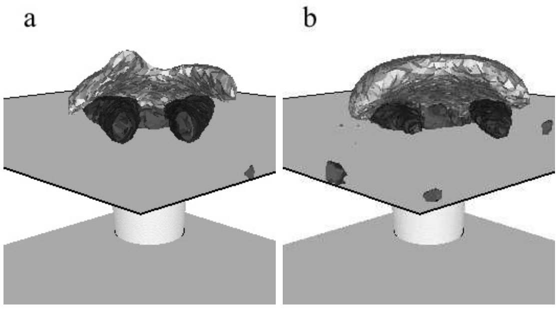

Figure 10: Visualization of the jet structure: front view. Iso-surface of the Q-criterion (dark grey) and of streamwise momentum (light grey). **a**: isothermal case. **b**: anisothermal case.

vortex pair (CVP). The counter-rotating vortices originate at the edges of the hole exit. More downstream, they get closer and are located under the jet core.

The vortices are seen thanks to an iso-surface of the Q-criterion (Hunt *et al.*, 1988), displayed in dark-grey in Fig. 9, which shows views of the CVP in the isothermal (Fig. 9a,b) and anisothermal (Fig. 9c,d) cases. The CVP in the isothermal calculation is stronger and can be observed further in the wake. It penetrates slightly more in the main flow, while the CVP in the anisothermal configuration is more parallel to the wall. Another difference is the distance between the vortices: $2.4\,d$ downstream of the aperture center, the distance between the two vortices of the CVP is suddenly decreased in the isothermal case. For the anisothermal case (Fig. 9c), the phenomenon cannot be observed. A front view of the jet organization is shown in Fig. 10, with the dark grey iso-surface of Q-criterion and an iso-surface of streamwise momentum representing the jet core. With a weaker CVP (Fig. 10b), the jet is wider. Indeed the jet penetration is also less important in the anisothermal case. This is consistent with the investigations of Peterson and Plesniak (2002), who showed that the intensity of the CVP can be directly related to film-cooling performance: in the case of a normal aperture, they showed that a strong CVP increases the jet penetration and decreases the lateral spreading, inducing a reduction of the cooling efficiency.

Peterson and Plesniak (2002) relate the strength of the CVP to the vorticity in the aperture. A counter-rotating vortex pair is present in the aperture and it interacts with the CVP. Depending on the direction of rotation and the intensity of the in-hole vortices, the CVP is differently affected: a vortex pair rotating in the same direction as the CVP reinforces it, while a vortex pair rotating in the hole in the opposite direction weakens the CVP. The dynamics of the flow in the aperture is thus studied, to investigate if the in-hole vortical structures are related to the CVP behavior. Figure 11 shows views of a cutting plane located at half the height of the hole and normal to the hole axis. The vorticity in the hole direction is displayed, and velocity vectors are shown. A white iso-line of momentum equal to $(\rho V)_{jet}$ is displayed to locate the jetting region. The vorticity is scaled by $V_{jet}/d \approx 1.4 \times 10^5$. In both cases, the vorticity field shows the presence of two pairs of counter-rotating vortices, one located near the lower wall (noted P1), and another one near the upper wall that rotates in the opposite direction (noted P2). P1 is directly related to the separation at the hole entrance and rotates in the same direction as the CVP. It is the main motion in the hole. P2 results from the aspiration of the boundary layer in the suction side,

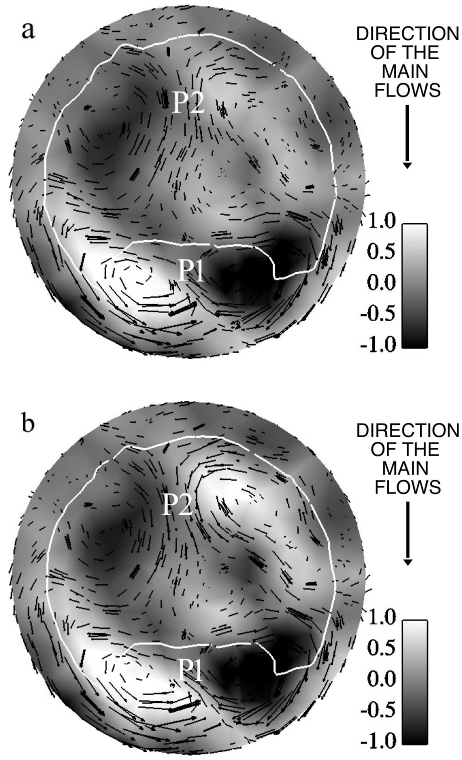

Figure 11: Vorticity in the direction of the hole over a cutting plane orthogonal to the hole axis and velocity vector. White iso-line: momentum magnitude equal to $(\rho V)_{jet}$. **a**: isothermal case. **b**: anisothermal case.

which already contains vortical motions (see MacManus and Eaton (2000) for the description of the vortical field downstream of a suction hole). P1 does not seem affected by the density variations: the maximum intensity of the vortices is approximately $\pm\,1.9$ in both cases. On the contrary, the vortical intensity of P2 is higher in Fig. 11b: approximately $\pm\,0.9$ for the anisothermal case and $\pm\,0.6$ for the isothermal case (Fig. 11a). Consistently with the conclusions of Peterson and Plesniak, it is possible that P2, that rotates in the direction opposite to the CVP, is responsible for the weakening of the CVP. P2 is more intense in the anisothermal case from the hole inlet: indeed the aspired streamwise vortices present on the suction side have a higher life duration. However the reasons for this persistence are not understood yet. The density gradients encountered by the flow in the thermal boundary that develops in the suction side may sustain the vortical motion: for instance, Eames and Hunt (1997) showed analytically how a particle of fluid experiences a lift force when it moves perpendicularly to a density gradient. Investigations are in progress to determine the exact causes of this phenomenon.

CONCLUSION

A method was recently proposed to perform simulations of full-coverage film cooling (FCFC) configurations using a computational domain periodic along the directions tangential to the perforated plate. This method was validated by comparison with experimental data (Mendez *et al.*, 2006a) in the case of a large-scale isothermal plate (Miron, 2005).

In the present paper, the isothermal method was extended to allow the computation of realistic FCFC configurations, including a high temperature difference across the perforated plate. A Large-Eddy Simulation of the flow around a periodic perforated plate is performed and the characteristics of the aerodynamical and thermal behavior of the flow are described.

Our anisothermal calculations allow to get detailed data about thermal behavior of the flow, especially locally resolved maps of heat transfers at the perforated plate. In the presented anisothermal computation, the heat flux in the aperture represents approximately 30 % of the total cooling heat flux (suction side + aperture). This confirms that a significant part of the plate cooling is done thanks to convection inside the aperture. It also suggests that an improvement of the calculation results would certainly be obtained by coupling the resolution of the flow with the resolution of the thermal field inside the plate. Besides, as shown by recent publications (see Errera and Chemin, 2004, Zhong and Brown, 2007), the current trend is to develop such methods to increase to predictive capacity of numerical tools for film cooling flows.

Comparisons of the anisothermal results with the isothermal calculations show that the general topology of the flow is not fundamentally modified due to density variations: the cooling fluid separates at the hole inlet, and the jet shows a characteristic kidney shape. The blowing ratio is high enough to make the jet separate at the outlet. In the injection side, a counter-rotating vortex pair is formed at the hole edges. This CVP, responsible for the entrainment of incident flow towards the wall, has a streamwise orientation and is located under the jet core downstream of the hole exit.

By comparing the flow in an isothermal and in an anisothermal cases, for the same geometrical configuration, differences in the vortical motions have been shown. In the suction side, the vortices created downstream of the hole inlet (MacManus and Eaton, 2000) have a higher life duration in the anisothermal simulation. The flow in the aperture is thus different: two pairs of vortices exist in the aperture, but the pair rotating in the direction opposite to the CVP is more intense in the anisothermal case. This also seems to have an impact when the jet issues on the injection side. The CVP is less intense in the anisothermal calculation, leading to a wider jet located closer from the wall.

ACKNOWLEDGMENTS

The authors are grateful to the European Community for funding this work under the project INTELLECT-DM (Contract No. FP6 - AST3 - CT - 2003 - 502961), and to the CINES and the BSC (Barcelona Supercomputing Center) for the access to supercomputer facilities.

REFERENCES

Champion, J.-L., Di Martino, P., Coron, X., 2005, "Influence of Flow Characteristics on the Discharge Coefficient of a Multiperforated Wall", In *ASME TURBO EXPO 2005, June 6-9, 2005, Reno-Tahoe, Nevada USA.*

Colin, O., and Rudgyard, M., 2000, "Development of high-order Taylor-Galerkin schemes for unsteady calculations", *J. Comput. Phys.*, Vol. 162(2), pp 338–371.

Eames, I., and Hunt, J. C. R., 1997, "Inviscid flow around bodies moving in weak density gradients without buoyancy effects", *J. Fluid Mech.*, Vol 353, pp 331–355.

Errera, M. P., and Chemin, S., 2004, "A Fluid-Solid Thermal Coupling Applied To An Effusion Cooling System", In *34th Fluid Dynamics Conference and Exhibit. Portland, Oregon.*

Gustafsson, K. M. B., 2001, "Experimental Studies of Effusion Cooling", Ph.D. thesis, Chalmers University of Technology, Göteborg.

Hunt, J. C. R., Wray, A. A., and Moin, P., 1988, "Eddies, streams, and convergence zones in turbulent flows", In *Proc. Summer Program CTR, NASA Ames - Stanford University.*

Iourokina, I. V., and Lele, S. K, 2006, "Large eddy simulation of film-cooling above the flat surface with a large plenum and short exit holes", In *44th Aerospace Sciences Meeting and Exhibit.*

Lefebvre, A. H., 1999, "Gas Turbines Combustion", Taylor & Francis.

MacManus, D. G., and Eaton, J. A., 2000, "Flow physics of discrete boundary layer suction measurements and predictions", *J. Fluid Mech.*, Vol. 417, pp 47–75.

Mendez, S., Nicoud, F., and Poinsot, T., 2006a, "Large-Eddy Simulations of a Turbulent Flow around a Multi-Perforated Plate", in *Complex effects in LES*, Vol. 56, pp. 289–303.

Mendez, S., Eldredge, J., Nicoud, F., Poinsot, T., Shoeybi, M., and Iaccarino, G., 2006b, "Numerical investigation and preliminary modeling of a turbulent flow over a multi-perforated plate", Center for Turbulence Research, in *Proceedings of the Summer Program 2006.*

Miron, P., 2005, "Étude expérimentale des lois de parois et du film de refroidissement produit par une zone multiperforée sur une paroi plane", Ph.D. Thesis, Université de Pau et des Pays de l'Adour.

Nicoud, F., and Ducros, F., 1999, "Subgrid-scale stress modelling based on the square of the velocity gradient tensor". *Flow, Turbulence and Combustion*, Vol. 62(3), pp 183-200.

Peterson, S. D., and Plesniak, M. W., 2002, "Short-hole jet-in-crossflow velocity field and its relationship to film-cooling performance", *Exps Fluids*, Vol. 33, pp 889–898.

Prière, C., Gicquel, L., Kaufmann, A., Krebs, W., and Poinsot, T., 2004, "LES predictions of mixing enhancement for jets in cross-flows", *J. of Turbulence*, Vol. 5, pp 005.

Renze, P., Meinke, M., and Shröder, W., 2006 "LES of turbulent mixing in film cooling flows", In *Conference on Turbulence and Interactions TI2006, May 29 - June 2, 2006, Porquerolles, France.*

Rouvreau, S., 2001 "Etude expérimentale de la structure moyenne et instantanée dun film produit par une zone multiperforée sur une paroi plane", Ph.D. thesis, ENSMA et Faculté des Sciences Fondamentales et Appliquées, Poitiers.

Schmitt, P., Poinsot, T., Schuermans, B., and Geigle, K., 2007, "Large-eddy simulation and experimental study of heat transfer, nitric oxide emissions and combustion instability in a swirled turbulent high-pressure burner", *J. Fluid Mech.*, Vol. 570, pp. 17–46.

Schönfeld, T., and Rudgyard, M., 1999, "Steady and unsteady flows simulations using the hybrid flow solver AVBP", *AIAA Journal*, Vol. 37, No. 11, pp. 1378–1385.

Tyagi, M., and Acharya, S., 2003, "Large eddy simulation of film cooling flow from an inclined cylindrical jet", *ASME J. Turbomach.*, Vol. 125, pp 734-742.

Yavuzkurt, S., Moffat, R. J., and Kays, W. M, 1980, "Full coverage film cooling. Part 1. Three-dimensional measurements of turbulent structures", *J. Fluid Mech.*, Vol. 101, pp 129-158.

Zhong, F., and Brown, G. L., 2007, "A 3-dimensional, coupled, DNS, heat transfer model and solution for multi-hole cooling", *Int. J. of Heat and Mass Transfer*, Vol. 50, pp 1328–1343.